Photo-Triggered Release of Caged Camptothecin Prodrugs from Dually Responsive Shell Cross-Linked Micelles

ARTICLE *in* MACROMOLECULES · AUGUST 2013

Impact Factor: 5.8 · DOI: 10.1021/ma400691j

5 AUTHORS, INCLUDING:

Xianglong Hu
South China Normal University
19 PUBLICATIONS **474** CITATIONS
SEE PROFILE

Tao Liu
University of Science and Technology of China
25 PUBLICATIONS **797** CITATIONS
SEE PROFILE

Guoying Zhang
University of Science and Technology of China
32 PUBLICATIONS **750** CITATIONS
SEE PROFILE

Macromolecules

Article

pubs.acs.org/Macromolecules

Photo-Triggered Release of Caged Camptothecin Prodrugs from Dually Responsive Shell Cross-Linked Micelles

Xianglong Hu,[†] Jie Tian,[‡] Tao Liu,[†] Guoying Zhang,[†] and Shiyong Liu*[,†]

[†]CAS Key Laboratory of Soft Matter Chemistry, Department of Polymer Science and Engineering, Hefei National Laboratory for Physical Sciences at the Microscale, University of Science and Technology of China, Hefei, Anhui 230026, China

[‡]Engineering and Materials Science Experiment Center, University of Science and Technology of China, Hefei 230027, China

Supporting Information

ABSTRACT: We report on the fabrication of dynamic covalent shell cross-linked (SCL) micelles with hydrophobic cores conjugated with photocaged chemotherapeutic drugs and coronas functionalized with ligands for tumor cell targeting. Two types of amphiphilic diblock copolymers, P(CL-*g*-CPT)-*b*-P(OEGMA-*co*-MAEBA)-CPT and PCL-*b*-P(OEGMA-*co*-MAEBA-*co*-FA), were synthesized via the combination of ring-opening copolymerization (ROP) of ε-caprolactone (CL) and 2-bromo-ε-caprolactone (CL-Br), atom transfer radical polymerization (ATRP) of oligo(ethylene glycol) monomethyl ether methacrylate (OEGMA) and *p*-(methacryloxyethoxy) benzaldehyde (MAEBA) comonomers, and "click" post-functionalization with photocaged camptothecin (CPT) prodrug and alkynyl-functionalized folic acid (FA) moieties, respectively. Mixed micelles coassembled from PCL-*b*-P(OEGMA-*co*-MAEBA-*co*-FA) and P(CL-*g*-CPT)-*b*-P(OEGMA-*co*-MAEBA)-CPT possess hydrophobic cores conjugated with photocaged CPT prodrugs and hydrophilic outer coronas covalently attached with aldehyde groups and FA moieties for subsequent shell cross-linking and cancer cell targeting. Shell cross-linking was performed at pH 6.2 upon addition of difunctional cross-linker, dithiol bis(propanoic dihydrazide) (DTP), under the catalysis of aniline. The obtained FA-decorated SCL micelles contain acylhydrazone and disulfide linkages in the outer coronas, which can be de-cross-linked under two biologically relevant conditions, mildly acidic or reductive microenvironments, that is, endosomal/lysosomal pH or high GSH level in the cytosol. The cleavage of caged CPT drug within the cores of SCL micelles can be effectively actuated under photo irradiation, whereas its diffusion out of micellar nanocarriers can be further modulated by pH and thiol levels due to the dually responsive nature of DTP cross-linker. Compared with the control, FA-decorated SCL micelles can more efficiently enter folate-receptor expressing cancer cells than folate-receptor deficient ones. Cell viability assays revealed that SCL micelles displayed at least ~9.7-fold enhanced cytotoxicity upon light irradiation. The reported targeting ligand decorated and prodrug-conjugated dynamic covalent SCL micelles exert intricate control concerning micellar stability, cancer cell targeting, photo-triggered parent drug release with photoactivated cytotoxicity, and tunable drug release profiles. All of these augur well for their potential application as a novel integrated platform for targeted drug delivery in cancer chemotherapy.

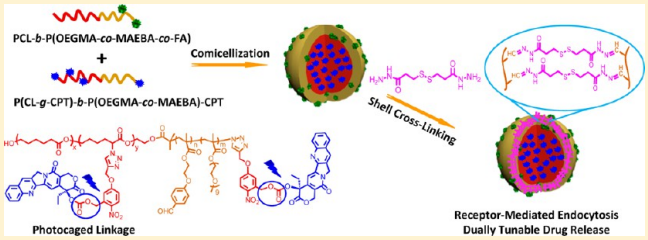

INTRODUCTION

In the past few decades, tremendous progress has been made in the field of polymeric drug delivery systems for cancer chemotherapy, partially due to key limitations associated with small molecule chemotherapeutic drugs, e.g., poor water solubility, limited stability, unsatisfactory biodistribution and pharmacokinetics, and severe side effects. Novel strategies have been explored by physically encapsulating small chemotherapeutic drugs into polymer matrix and polymeric assemblies (e.g., micelles and vesicles) to achieve enhanced water solubility, improved drug loading capacity, sustained controlled release and prolonged blood circulation duration. For instance, amphiphilic block copolymers are utilized to fabricate nanocarriers with core−shell nanostructures encapsulating hydrophobic anticancer drugs in the cores. However, the simple physical encapsulation of drugs within polymeric assemblies suffers from severe disadvantages such as relatively low drug loading content and loading efficiency, and unavoidable premature drug release during storage and blood circulation.[1,2]

Although shell or core cross-linking (SCL or CCL) of polymeric micelles and vesicles can considerably enhance their structural stability, and the integration of core or corona stimuli-responsiveness can lead to triggered or programmed release,[3] the premature release of physically encapsulated drugs, typically with low loading content, is still unavoidable.[4−13] To circumvent these drawbacks, polymer-drug conjugates show great promises.[14−16] A variety of strategies have been utilized to covalently anchor chemotherapeutic drugs onto polymer backbones and side chains via cleavable or degradable linkages.

Received: April 6, 2013
Revised: July 5, 2013
Published: July 22, 2013

Scheme 1. Schematics for the Fabrication of Shell Cross-Linked (SCL) Micelles from P(CL-*g*-CPT)-*b*-P(OEGMA-*co*-MAEBA)-CPT and PCL-*b*-P(OEGMA-*co*-MAEBA-*co*-FA) Amphiphilic Diblock Copolymers[a]

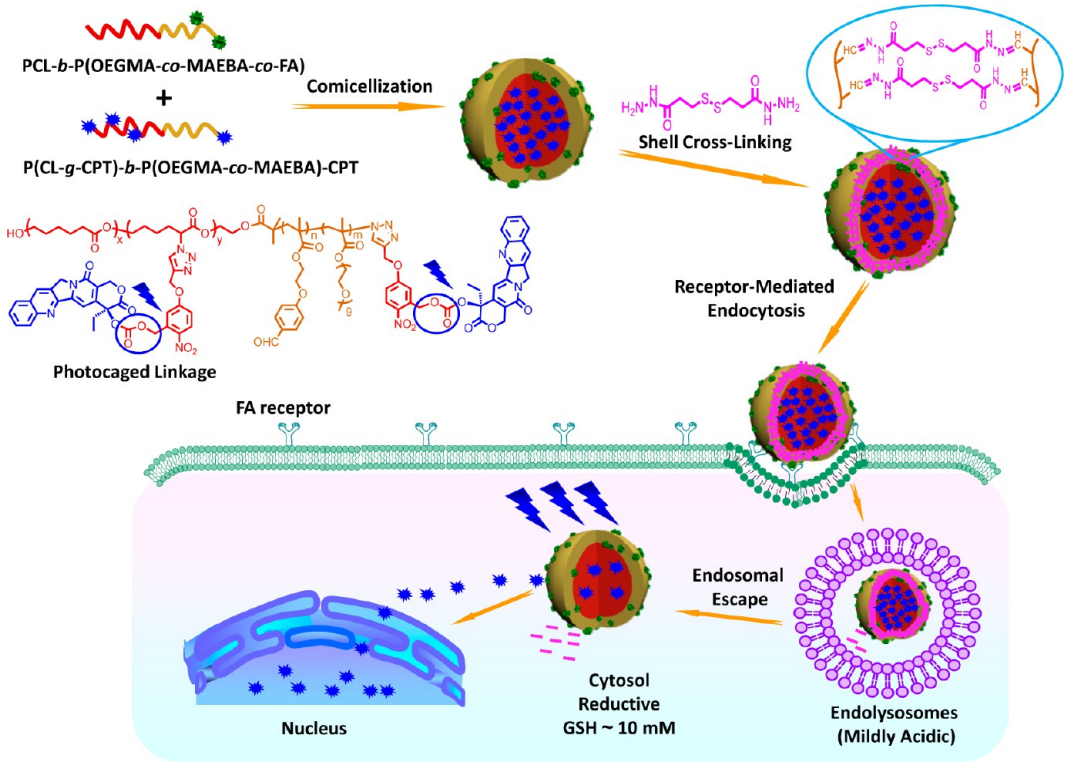

[a]Micellar coronas are functionalized with targeting ligands, folic acid (FA), and micellar cores are conjugated with caged camptothecin (CPT) prodrug moieties. The cleavage of caged CPT drug within the cores of SCL micelles can be effectively actuated under photoirradiation, whereas its diffusion out of micellar nanocarriers can be further modulated by pH and thiol levels due to the dually responsive nature of cross-linkers.

Among these, photocaged linkages have been broadly applied to construct polymer−drug conjugates due to that the effective release of active drugs can be achieved with excellent spatial and temporal precision upon light irradiation.[17−19] In consideration of these advantages, photoactivatable prodrugs are not only suitable for surface cancer treatment, but also applicable to deep-seated cancers under the guidance of endoscopes or optical fibers, which are also used for photodynamic therapy.[20]

Among a variety of photocaging strategies that have been investigated, *o*-nitrobenzyl derivatives, pioneered by Schofield and Woodward,[21,22] have gained tremendous attention in the field of synthetic polymer-drug conjugates.[23] For example, Nishimoto and co-workers synthesized a series of anticancer prodrugs, 2-nitrobenzyl-functionalized 5-fluorouracil (5-FU) prodrug with photoactivatable antitumor properties.[24] Later, Rotello et al. reported the synthesis of gold nanoparticles functionalized with photocaged 5-FU, demonstrating light-controlled release of active 5-FU and light-activated cytotoxicity.[25] Besides, Choi's and Hartman's research group also utilized *o*-nitrobenzyl caging group to design photocaged doxorubicin (DOX), which exhibited light-controlled release of DOX.[26,27] Recently, Grubbs, Tirrell and their co-workers covalently attached chemotherapeutic drugs (DOX or camptothecin) onto bottle-brush polynorbornene-PEG polymers via photo-cleavable *o*-nitrobenzyl ester linkages.[28,29] In addition to the above examples concerning *o*-nitrobenzyl photocaged chemotherapeutic drugs, other active substances with varying functions, such as proteins,[30,31] targeting ligands,[32] oligonucleotides,[33] fluorescent dyes,[34,35] and amino acids[36] have also been involved for photocaging.

Another aspect which needs to be considered is how to deliver drug nanocarriers in a tissue- and cell-specific manner. Currently, all of clinically validated drug delivery systems based on therapeutic and imaging nanoparticles utilize the passive targeting strategy.[37] The majority of these nanocarriers exhibit prolonged circulation times *in vivo* and accumulate at a particular site simply due to blood hemodynamic forces and diffusive mechanisms. Passive targeting is widely exploited in anticancer applications due to that tumors facilitate accumulation of theranostic nanoparticles through the widely recognized "enhanced permeation and retention" (EPR) effect, which was first proposed by Maeda et al. in 1980s.[38] Many passively targeted drug delivery systems possess a hydrophilic surface coated with PEG brushes for biocompatibility; however this highly hydrophilic surface does not result in effective endocytic uptake by cancer cells. The so-called "PEG dilemma" can severely hamper efficient drug delivery into tumor cells.[39]

To overcome these problems existing in passive targeting, targeted polymeric drug delivery systems have been used for more efficient tumor retention and cellular uptake, thereby resulting in improved therapeutic efficacy. Active targeting that uses specific ligands including monoclonal antibodies, peptides, and aptamers that bind to specific proteins or surface antigens overexpressed on cancer cells is a practical and attractive approach. Among these ligands, folic acid (FA), a low-molecular weight vitamin, plays an irreplaceable role in cell survival and binds with high affinity to the folate receptor, which is a membrane-anchored protein overexpressed in many cancer cell surfaces and can serve as a tumor marker.[40,41]

dx.doi.org/10.1021/ma400691j | *Macromolecules* 2013, 46, 6243−6256

Finally, camptothecin (CPT) and its derivatives are effective chemotherapeutic drugs, though their full clinical potentials have yet to be explored due to intrinsic limitations, such as the lack of water solubility, hydrolysis of pharmacologically active lactone rings, and fast nonspecific biodistribution within the whole body.[42,43] Thus, it is imperative to develop nanocarriers for the targeted delivery and controlled release of CPT drugs. On the other hand, CPT is a cytotoxic quinoline alkaloid that inhibits the type I topoisomerase through hydrogen bonding interactions with the participation of hydroxyl group at position 20. Thus, the reaction of hydroxyl group with the *o*-nitrobenzyl-protecting moiety will afford CPT prodrug with caged anticancer capabilities.

In this work, we envisaged that FA-functionalized dually responsive SCL micelles covalently conjugated with *o*-nitrobenzyl photocaged CPT prodrug in the hydrophobic cores might serve as an effective targeted delivery platform (Scheme 1). Accordingly, we synthesized two types of amphiphilic diblock copolymers, PCL-*b*-P(OEGMA-*co*-MAEBA-*co*-FA) containing FA moieties in the hydrophilic block and P(CL-*g*-CPT)-*b*-P(OEGMA-*co*-MAEBA)-CPT conjugated with photocaged CPT prodrug in the hydrophobic block (Schemes 2 and 3). Upon comicellization, shell cross-linking was achieved upon the introduction of difunctional cross-linker, dithiolbis(propanoic dihydrazide) (DTP). The obtained FA-decorated SCL micelles, which are conjugated with photocaged chemotherapeutic drug in micellar cores, contain acylhydrazone and disulfide linkages in micellar coronas, which can be de-cross-linked via two biologically relevant milieu, acidic or reductive conditions. Thus, upon photoactivation of CPT prodrugs, their diffusion out of micellar nanocarriers can be further modulated by external pH and thiol levels (Scheme 1). Moreover, in order to interrogate whether the presence of FA targeting ligands will alter cellular uptake and cytotoxicity features against folate-receptor expressing/deficient cancer cells, FA-free SCL micelles were utilized as the control. Finally, the endsosomal escaping capability of FA-decorated SCL micelles, phototriggered CPT parent drug release, and photoactivated cytotoxicity were also explored.

Scheme 2. Synthetic Schemes Employed for the Preparation of Photocaged CPT Prodrug, 2-Nitro-5-propargyloxybenzyl Carbonate Camptothecin (NBCCPT)

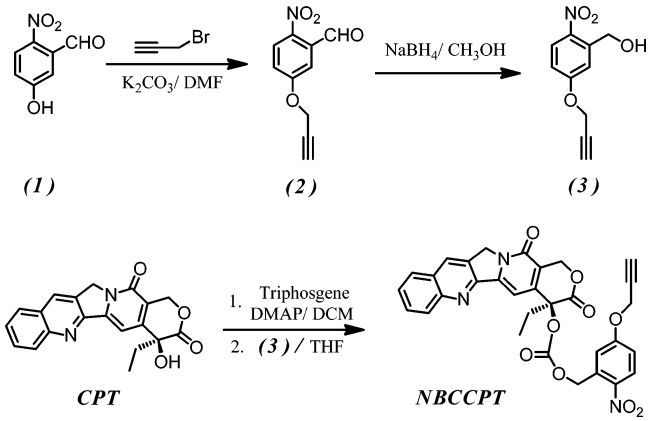

EXPERIMENTAL SECTION

Materials. Oligo(ethylene glycol) monomethyl ether methacrylate (OEGMA, M_n = 475 g/mol, mean degree of polymerization, DP, is 8–9) purchased from Aldrich was passed through a neutral alumina column to remove the inhibitor and then stored at −20 °C prior to use. *ε*-Caprolactone (CL, 99%, Acros) was dried over calcium hydride (CaH_2) and distilled under reduced pressure before use. *N*,*N*,*N*′,*N*″,*N*″-Pentamethyldiethylenetriamine (PMDETA, 98%), copper(I) bromide (CuBr, 98%), stannous(II) octanoate ($Sn(Oct)_2$, 95%), dithiothreitol (DTT), 3-(4,5-dimethylthiazol-2-yl)-2,5-diphenyltetrazolium bromide (MTT), camptothecin (CPT) were purchased from Aldrich and used as received. Tris(2-carboxyethyl)phosphine hydrochloride (TCEP) was obtained from Alfa Aesar and used without further purification. Fetal bovine serum (FBS), penicillin, streptomycin, and Dulbecco's modified Eagle's medium (DMEM) were purchased from GIBCO and used as received. Toluene was dried by refluxing over sodium shavings and distilled just prior to use. Aniline was distilled and stored at −4 °C under N_2 atmosphere. Tetrahydrofuran (THF), dimethylfomamide (DMF), dichloromethane (DCM), diethyl ether, and all other reagents were purchased from Sinopharm Chemical Reagent Co. Ltd. and used as received. Water used in this study was deionized with a Milli-QSP reagent water system (Millipore) to a specific resistivity of 18.4 MΩ·cm. 2-Nitro-5-propargyloxybenzyl alcohol,[44] *p*-(methacryloxyethoxy)benzaldehyde (MAEBA),[8] 2-bromo-*ε*-caprolactone (CL-Br),[45] 2-hydroxyethyl 2-bromo-2-methylpropanoate (HBMP),[46] 3-azidopropyl methacrylate (AzPMA),[47] alkynyl-functionalized folic acid (*alkynyl*-folate),[48] and 4-(2-methylacryloy-loxyethylamino)-7-nitro-2,1,3-benzoxadiazole (NBDMA)[49] were synthesized according to literature procedures.

Sample Preparation. Synthetic routes employed for the preparation of photocaged CPT prodrug, NBCCPT, and amphiphilic diblock copolymers, P(CL-*g*-CPT)-*b*-P(OEGMA-*co*-MAEBA)-CPT and PCL-*b*-P(OEGMA-*co*-MAEBA-*co*-FA) are shown in Schemes 2 and 3.

Synthesis of Photocaged CPT Prodrug (NBCCPT). NBCCPT was synthesized according to previous literature reports with slight modifications (see Scheme 2).[29] CPT (0.8 g, 2.3 mmol) and DMAP (0.84 g, 6.9 mmol) were suspended in DCM under N_2 atmosphere. Triphosgene (0.27 g, 0.92 mmol) was introduced and the mixture was stirred for 30 min at room temperature. 2-Nitro-5-propargyloxybenzyl alcohol (**3**) (0.57 g, 2.76 mmol, in 10 mL of dry THF) was added dropwise under N_2 atmosphere. The reaction mixture was stirred overnight in dark and a precipitate formed during this stage. The mixture was then diluted with EtOAc (100 mL) and washed once with water (50 mL), and once with brine (50 mL). The organic layer was collected and dried over anhydrous $MgSO_4$, filtered, and concentrated on a rotary evaporator. The solid residues were purified by column chromatography (100% EtOAc, TLC $R_f \sim 0.5$) to afford NBCCPT as a colorless solid (1.22 g, 89%). The chemical structure of NBCCPT was verified by ^{1}H NMR (Figure S1, Supporting Information), and ^{13}C NMR and ESI–MS analysis (Figure S2).

Synthesis of HO-P(OEGMA-co-MAEBA) Macroinitiator (Scheme 3). HBMP (32.0 mg, 0.152 mmo1), OEGMA (5.94 g, 12.5 mmol), MAEBA (1.55 g, 6.60 mmol), PMDETA (26.0 mg, 0.152 mmol), and DMF (6 mL) were charged into a reaction flask. The mixture was degassed by three freeze–pump–thaw cycles and then CuBr (21.7 mg, 0.152 mmol) was introduced under N_2 protection. After thermostating at 60 °C in an oil bath and stirring for 10 h, the reaction tube was quenched into liquid N_2, opened and exposed to air, and diluted with 30 mL of THF. The mixture was then passed through a silica gel column using THF as the eluent to remove copper catalysts. After all the solvents were removed on a rotary evaporator, the residues were dissolved in THF and precipitated into an excess of cold diethyl ether. The above dissolution–precipitation cycle was repeated for three times. The final product was dried in a vacuum oven overnight at room temperature, yielding a colorless viscous solid (5.2 g, yield: 69.3%). The molecular weight and molecular weight distribution of *HO*-P(OEGMA-*co*-MAEBA) were determined by GPC using THF as the eluent, revealing an M_n of 25 600 and an M_w/M_n of 1.21 (Figure 1a). The conversion of OEGMA and MAEBA was determined to be 54.6% and 62.2%, respectively based on ^{1}H NMR analysis of the crude product before purification. Because of the overlapping of resonance signals characteristic of OEGMA and MAEBA residues within the final

dx.doi.org/10.1021/ma400691j | *Macromolecules* 2013, 46, 6243–6256

Scheme 3. Schematic Illustration for the Synthesis of P(CL-*g*-CPT)-*b*-P(OEGMA-*co*-MAEBA) Amphiphilic Diblock Copolymer Conjugated with Photocaged CPT Prodrug and PCL-*b*-P(OEGMA-*co*-MAEBA-*co*-FA) Amphiphilic Diblock Copolymer Functionalized with FA in the Hydrophilic Block

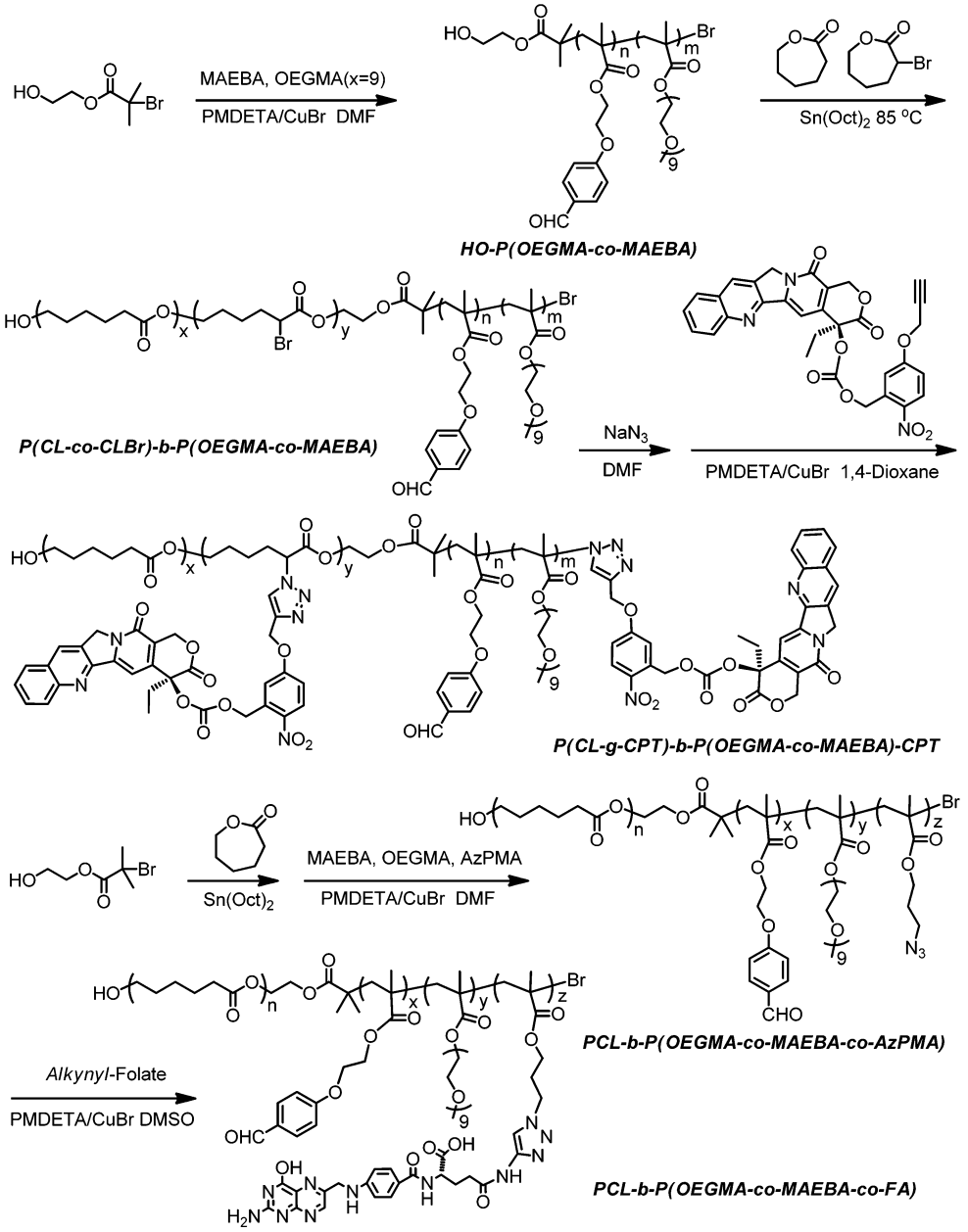

polymer, this represents the best estimation of the relative contents of two monomers in the copolymer. In combination with the M_n data determined from GPC, the chemical structure of the product was determined to be *HO*-P(OEGMA$_{0.62}$-*co*-MAEBA$_{0.38}$)$_{72}$ and shortened as *HO*-P(OEGMA-*co*-MAEBA) in subsequent sections.

Synthesis of P(CL-co-CLBr)-b-P(OEGMA-co-MAEBA) Diblock Copolymer. The amphiphilic diblock copolymer, P(CL-*co*-CLBr)-*b*-P(OEGMA-*co*-MAEBA), was synthesized via the ROP of CL and CL-Br using *HO*-P(OEGMA-*co*-MAEBA) as the macroinitiator. Typically, *HO*-P(OEGMA-*co*-MAEBA) (4.50 g, 0.17 mmol), CL-Br (1.97 g, 10.2 mmol), CL (1.16 g, 10.2 mmol), and dry toluene (15 mL) were charged into a glass ampule equipped with a magnetic stirring bar. About 5 mL toluene was removed under reduced pressure at first. Then a 0.7 mL solution of Sn(Oct)$_2$ in toluene (0.1 mol/L) was added under nitrogen protection. After another 5 mL of toluene was removed under reduced pressure, the glass ampule was carefully sealed under vacuum and stirred at 85 °C for 24 h. The reaction tube was quenched into liquid N_2 and exposed to air and the product diluted with THF and precipitated into an excess of diethyl ether. The above dissolution−precipitation cycle was repeated three times. The final product was dried in a vacuum oven overnight at room temperature to afford a brown solid (5.2 g, yield: 68.2%). The molecular weight and molecular weight distribution of P(CL-*co*-CLBr)-*b*-P(OEGMA-*co*-MAEBA) diblock copolymer were determined by GPC using THF as the eluent, revealing an M_n of 32,300 and an M_w/M_n of 1.27 (Figure 1b). The molar fraction of CL in the P(CL-*co*-CLBr) block was determined to be 0.43 by ^{1}H NMR analysis (Figure 2b). Thus, the polymer was denoted as P(CL$_{0.43}$-*co*-CLBr$_{0.57}$)$_{64}$-*b*-P(OEGMA$_{0.62}$-*co*-MAEBA$_{0.38}$)$_{72}$ and shortened as (PCL-*co*-CLBr)-*b*-P(OEGMA-*co*-MAEBA) in subsequent sections.

Synthesis of P(CL-g-CPT)-b-P(OEGMA-co-MAEBA)-CPT Diblock Copolymer. The amphiphilic diblock copolymer P(CL-*g*-CPT)-*b*-P(OEGMA-*co*-MAEBA)-CPT was obtained via the click reaction of alkynyl-functionalized photocaged prodrug, NBCCPT, with the

dx.doi.org/10.1021/ma400691j | *Macromolecules* 2013, 46, 6243−6256

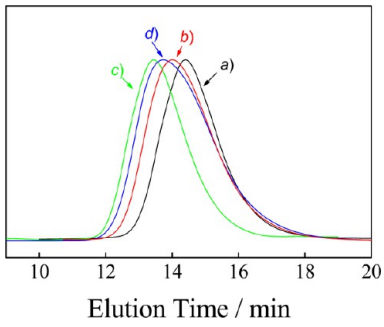

Figure 1. THF GPC traces recorded for (a) HO-P(OEGMA-*co*-MAEBA) (M_n = 25.6 kDa, M_w/M_n = 1.21), (b) P(CL-*co*-CLBr)-*b*-P(OEGMA-*co*-MAEBA) (M_n = 32.3 kDa, M_w/M_n = 1.27), (c) P(CL-*g*-CPT)-*b*-P(OEGMA-*co*-MAEBA)-CPT (M_n = 42.6 kDa, M_w/M_n = 1.20), and (d) PCL-*b*-P(OEGMA-*co*-MAEBA-*co*-FA) (M_n = 37.2 kDa, M_w/M_n = 1.29).

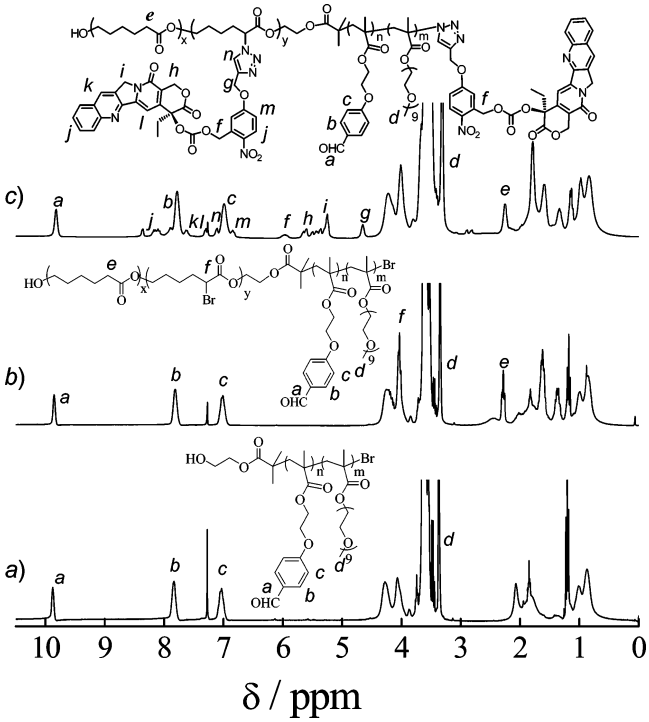

Figure 2. ^{1}H NMR spectra recorded in $CDCl_3$ for (a) HO-P(OEGMA-*co*-MAEBA) precursor, (b) P(CL-*co*-CLBr)-*b*-P(OEGMA-*co*-MAEBA), and (c) P(CL-*g*-CPT)-*b*-P(OEGMA-*co*-MAEBA)-CPT diblock copolymers.

azidation product of P(CL-*co*-CLBr)-*b*-P(OEGMA-*co*-MAEBA). First, sodium azide (1.32 g, 20.35 mmol), P(CL-*co*-CLBr)-*b*-P(OEGMA-*co*-MAEBA) (4.00 g, 0.11 mmol), and DMF (15 mL) were charged into a glass ampule equipped with a magnetic stirring bar. After being stirred for 24 h at room temperature, the mixture was passed through a silica gel column using THF as the eluent to remove insoluble salts. After removing most of the solvents on a rotary evaporator, the mixture was precipitated into an excess of cold diethyl ether, then filtered. The residues were dissolved in THF and precipitated into an excess of diethyl ether. The above dissolution−precipitation cycle was repeated for three times. The final product was dried in a vacuum oven overnight at room temperature to afford a pale brown solid (3.1 g, yield: 77.5%). Thus, the polymer was denoted as $(PCL\text{-}g\text{-}N_3)_{64}$-*b*-$P(OEGMA_{0.62}\text{-}co\text{-}MAEBA_{0.38})_{72}$-$N_3$.

Subsequently, $(PCL\text{-}g\text{-}N_3)_{64}$-*b*-$P(OEGMA_{0.62}\text{-}co\text{-}MAEBA_{0.38})_{72}$-$N_3$ (1.90 g, 53.4 μmol), NBCCPT (1.15 g, 1.98 mmol), PMDETA (0.34 g, 1.98 mmol), and 1,4-dioxane (5 mL) were charged into a glass ampule equipped with a magnetic stirring bar. The mixture was degassed by three freeze−pump−thaw cycles, and then CuBr (0.28 g, 1.98 mmol) was introduced under nitrogen. After thermostatting at 45 °C in an oil bath and stirring for 24 h, the reaction tube was quenched into liquid N_2, opened and exposed to air, and diluted with 20 mL THF. The mixture was then passed through basic alumina column using THF as the eluent to remove copper catalysts. After removal of all the solvents on a rotary evaporator, the residues were dissolved in THF and precipitated into an excess of cold diethyl ether. The obtained solids were further purified by dialysis (cellulose membrane, molecular weight cutoff: 3500 Da) against deionized water for 24 h, and then lyophilized as a pale solid (2.20 g, yield: 72.1%). GPC analysis revealed an M_n of 42 600 and an M_w/M_n of 1.20 (Figure 1c). On the basis of ^{1}H NMR analysis (Figure 3), the molar ratio between

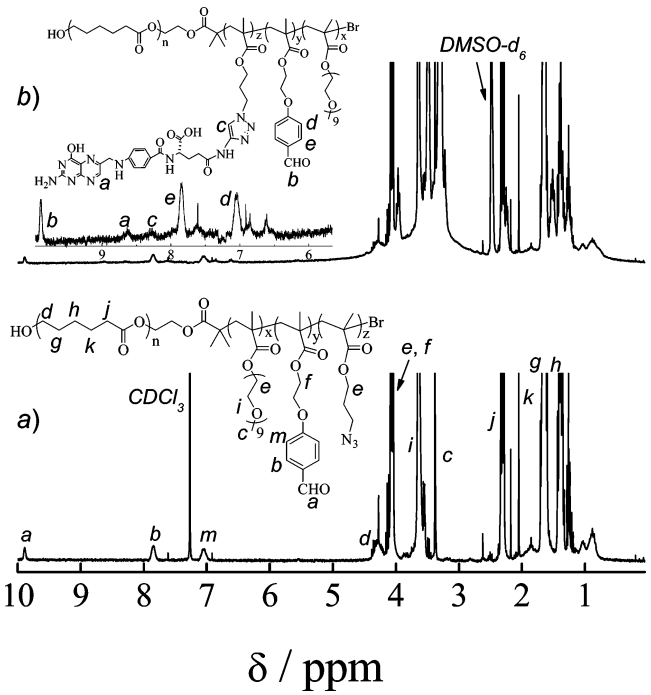

Figure 3. ^{1}H NMR spectra recorded for (a) PCL-*b*-P(OEGMA-*co*-MAEBA-*co*-AzPMA) and (b) folic acid functionalized PCL-*b*-P(OEGMA-*co*-MAEBA-*co*-FA) diblock copolymers in $CDCl_3$ and DMSO-d_6, respectively.

benzaldehyde and CPT moieties can be obtained. Thus, the polymer was denoted as $(PCL_{64}\text{-}g\text{-}CPT_{15})$-*b*-$P(OEGMA_{0.62}\text{-}co\text{-}MAEBA_{0.38})_{72}$-CPT and shortened as (PCL-*g*-CPT)-*b*-P(OEGMA-*co*-MAEBA)-CPT.

Synthesis of PCL-b-P(OEGMA-co-MAEBA-co-FA) Diblock Copolymer. First, PCL_{43}-Br was obtained via ROP of CL by employing HBMP as the initiator as reported previously.[8] Then PCL_{43}-Br was employed as ATRP macroinitiator to copolymerize MAEBA, OEGMA, and AzPMA due to its terminal bromine. Typically, PCL_{43}-Br (0.26 g, 0.05 mmol), OEGMA (1.90 g, 4.0 mmol), MAEBA (0.35 g, 1.5 mmol), AzPMA (42.3 mg, 0.25 mmol), PMDETA (8.7 mg, 0.05 mmol), and DMF (5 mL) were charged into a reaction flask. The mixture was degassed by three freeze−pump−thaw cycles and backfilled with nitrogen. After this was heated to 50 °C, CuBr (7.2 mg, 0.05 mmol) was introduced as a solid under the protection of N_2 to start the polymerization. After the reaction was stirred for 12 h, the reaction tube was quenched into liquid N_2, opened, and exposed to air and the product diluted with 10 mL of THF. The mixture was then passed through a silica gel column using THF as the eluent to remove copper catalysts. After most of the solvent was removed on a rotary evaporator, the residues were precipitated into an excess of cold diethyl ether. The above dissolution−precipitation cycle was repeated three times. The final product was dried in a vacuum oven overnight at room temperature, yielding a colorless viscous solid (1.43 g, yield:

dx.doi.org/10.1021/ma400691j | *Macromolecules* 2013, 46, 6243−6256

62.2%), and then stored at −20 °C prior to use. The conversion of OEGMA, MAEBA and AzPMA was determined to be 76.2%, 23.3%, 40%, respectively, based on ^{1}H NMR analysis of the crude product before purification. Combined with the M_n data from GPC, the chemical structure of the product was determined to be PCL_{43}-*b*-$P(OEGMA_{0.87}$-*co*-$MAEBA_{0.1}$-*co*-$AzPMA_{0.03})_{70}$.

In the second step, *alkynyl*-folate (0.13 g, 0.27 mmol), PCL_{43}-*b*-$P(OEGMA_{0.87}$-*co*-$MAEBA_{0.1}$-*co*-$AzPMA_{0.03})_{70}$ (1.20 g, 0.067 mmol azide moieties), PMDETA (11.6 mg, 0.067 mmol), and DMSO (10 mL) were charged into a glass ampule equipped with a magnetic stirring bar. The mixture was degassed by three freeze−pump−thaw cycles, and then CuBr (9.6 mg, 0.067 mmol) was introduced under nitrogen. After thermostating at 50 °C in an oil bath and the reaction stirred for 12 h, the reaction tube was quenched into liquid N_2, opened, and exposed to air and the product diluted with 30 mL of THF. The reaction mixture was then passed through a basic alumina column using THF as the eluent to remove copper catalysts. After removal of the solvents on a rotary evaporator, the residues were dissolved in THF and precipitated into an excess of cold diethyl ether. The obtained solid was further purified by dialysis (cellulose membrane, molecular weight cutoff: 3500 Da) against deionized water for 24 h and then lyophilized as a colorless solid (1.08 g, yield: 81.2%). GPC characterization revealed an M_n of 37 200 and an M_w/M_n of 1.29 (Figure 1d). UV−vis analysis in DMSO using folic acid as the calibration standard indicated the quantitative transformation of azide groups into folate moieties. Thus, the polymer was denoted as PCL_{43}-*b*-$P(OEGMA_{0.87}$-*co*-$MAEBA_{0.1}$-*co*-$FA_{0.03})_{70}$ and shortened as PCL-*b*-P(OEGMA-*co*-MAEBA-*co*-FA) in subsequent sections. Following similar procedures, NBD-labeled diblock copolymer, PCL_{43}-*b*-$P(OEGMA_{0.56}$-*co*-$MAEBA_{0.43}$-*co*-$NBD_{0.01})_{80}$, was also synthesized. The diblock copolymer was denoted as PCL-*b*-P(OEGMA-*co*-MAEBA-*co*-NBD) in subsequent sections.

Fabrication of FA-Decorated and Photocaged Drug Conjugated Shell Cross-Linked Micelles. The mixture of amphiphilic diblock copolymers (5 mg), PCL-*b*-P(OEGMA-*co*-MAEBA-*co*-FA) and P(CL-*g*-CPT)-*b*-P(OEGMA-*co*-MAEBA)-CPT (1/4, w/w), were molecularly dissolved in DMSO, then 40 mL of NH_4OAc buffer (50 mM, pH = 6.2) was added dropwise under vigorous stirring. After this was allowed to stand and equilibrate for 6 h, DMSO was removed by dialysis (cellulose membrane, molecular weight cutoff = 3500 Da) against NH_4OAc buffer (50 mM, pH = 6.2) for 24 h to afford 0.1 g/L noncross-linked (NCL) micelles. Shell cross-linking was actuated by introducing difunctional cross-linker DTP (DTP/MAEBA molar ratio 1:2) into 0.1 g/L aqueous solution of NCL micelles in the presence of 10 mM aniline. The resultant solution was stirred for 24 h at 25 °C and then dialyzed against deionized water for 24 h at pH 7.4 to remove unreacted cross-linker and the catalyst (aniline). DLS and Ellman's assay were employed to confirm the successful fabrication of FA-decorated SCL micelles conjugated with photocaged CPT drug. In addition, PCL-*b*-P(OEGMA-*co*-MAEBA-*co*-AzPMA) and P(CL-*g*-CPT)-*b*-P(OEGMA-*co*-MAEBA)-CPT diblock copolymer mixtures (1/4, w/w) were also used to prepare FA-free SCL micelles. For flow cytometry and additional confocal microscope colocalization experiments, FA-decorated and NBD-labeled SCL micelles were fabricated from a mixture of PCL-*b*-P(OEGMA-*co*-MAEBA-*co*-FA) and PCL-*b*-P(OEGMA-*co*-MAEBA-*co*-NBD) (1/1, w/w), whereas FA-free and NBD-labeled SCL micelles were fabricated from PCL-*b*-P(OEGMA-*co*-MAEBA-*co*-AzPMA) and PCL-*b*-P(OEGMA-*co*-MAEBA-*co*-NBD) diblock copolymers (1/1, w/w).

In Vitro Drug Release from FA-Decorated SCL Micelles. For the experimental setup, a disposable polypropylene dialysis cup with integrated, low-binding regenerated cellulose membranes of molecular weight cutoff of 2000 Da was employed.[50] Freeze-dried FA-decorated SCL micelles dispersed in 0.1 M phosphate buffer (pH = 7.4; pH = 5.0; pH = 7.4 with 10 mM DTT; pH = 5.0 with 10 mM DTT) were transferred into the dialysis cup, which was immersed in the same buffered solution and gently shaken at 37 °C. UV irradiation promoted drug cleavage and release was initiated when the dialysis cup was exposed to UV light. After various time intervals, aliquots of the external medium were withdrawn and replaced with the same volume of fresh buffer solution. The release rate of CPT was evaluated by means of HPLC analysis. The CPT conjugation/loading content (LC %) was calculated as

$$\mathrm{LC\%} = [W_{\mathrm{conjugated}}]/[W_{\mathrm{polymer}}] \times 100\%$$

LC%=$[W_{\mathrm{conjugated}}]/[W_{\mathrm{polymer}}] \times 100\%$where $W_{\mathrm{conjugated}}$, and W_{polymer} refer to the weight of conjugated CPT drug within micelles and the weight of diblock copolymer micelles, respectively. LC% was actually determined by the chemical structures of diblock copolymers and composition of diblock mixtures.

Cellular Uptake and Intracellular Localization of SCL Micelles. Cellular uptake and intracellular localization of SCL micelles were determined using confocal laser scanning microscopy (CLSM). A549 cells were plated onto glass bottom Petri dishes at a density of 80 000 cells per dish and then cultured in Dulbecco's modified Eagle medium (DMEM) supplemented with 10% fetal bovine serum (FBS), penicillin (100 units per mL), and streptomycin (100 μg mL^{-1}) for 24 h at 37 °C in CO_2/air (5:95). Cells were treated with FA-free or FA-decorated SCL micelles for 2 h at a final CPT concentration of 3 μg mL^{-1}. Then, the cells were washed with PBS buffer three times. The images were taken using a Leica TCS SP5 microscope. The fluorescence signal from CPT moieties was observed using a 405 nm laser with the emission channel set to be 415−470 nm. For colocalization test, Lysotracker Red was used to localize late endosomes and lysosomes. Lysotracker Red emission was observed using a 594 nm laser and the emission wavelength was set in the range 605−720 nm. A549 cells were first incubated with FA-decorated SCL micelles for 2 h to ensure sufficient cellular uptake, followed by UV irradiation for 15 min, and then incubation for another 2, 6, and 10 h. The intracellular distributions of SCL micelles were quantitatively evaluated by calculating the colocalization ratio of blue fluorescence pixels (from CPT moieties) or green fluorescence pixels (from NBD moieties) with Lysotracker Red pixels (red). Co-localization ratio of FA-decorated SCL micelles with late endosomes and lysosomes was quantified as

$$\text{co-localization ratio } \% = [\mathrm{pixel}_{\text{co-localization}}/\mathrm{pixel}_{\text{SCL micelles total}}] \times 100\%$$

where $\mathrm{pixel}_{\text{co-localization}}$ represents the number of SCL micelles pixels colocalizing with Lysotracker Red, and $\mathrm{pixel}_{\text{SCL micelles total}}$ represents the total number of pixels corresponding to SCL micelles within cells. All the results are presented as the mean value averaged from ∼20 cells.

For flow cytometric analysis, A549 cells were seeded into 24-well plates at 80,000 cells per well in 0.5 mL of complete DMEM and cultured at 37 °C in a 5% CO_2 humidified atmosphere for 24 h. After being treated with SCL micelles for 1 h at 4 or 37 °C, the cells were then rinsed twice with cold PBS, trypsinized, washed with cold PBS, and treated for 5 min with 0.2% trypan blue to quench the extracellular fluorescence. The cells were further washed with cold PBS, filtered through 35 μm nylon mesh, and subjected to analysis using a BD FACSCalibur flow cytometer with the excitation wavelength set to be 488 nm for NBD dye moieties.

In Vitro Cytotoxicity Assay. A549 cells were chosen as folate-receptor expressing cancer cells to evaluate the antitumor activity of FA-decorated SCL micelles via the MTT assay. A549 cells were first cultured in Dulbecco's modified Eagle medium (DMEM) supplemented with 10% fetal bovine serum (FBS), penicillin (100 units/mL), and streptomycin (100 μg mL^{-1}) at 37 °C in a CO_2/air (5:95) incubator for 2 days. For cytotoxicity assay, A549 cells were seeded in a 96-well plate at an initial density of ca. 5000 cells/well in 100 μL of complete DMEM medium. After this was incubated for 24 h, DMEM was replaced with fresh medium, and the cells were treated with SCL micellar solution at varying concentrations. After incubating for 4 h, phototriggered drug release was actuated under 365 nm UV irradiation for 15 min using a hand-held UV lamp. Then, the treated cells were incubated in a humidified environment with 5% CO_2 at 37 °C for 36 h. The MTT reagent (in 20 μL PBS, 5 mg/mL^{-1}) was added to each well. The cells were further incubated for 4 h at 37 °C. The medium in each well was then removed and replaced by 180 μL DMSO. The plate

was gently agitated for 15 min before the absorbance at 570 nm was recorded by a microplate reader (Thermo Fisher). Each experiment condition was done in quadruplicate, and the data are shown as the mean value plus a standard deviation (±SD).

Characterization. All nuclear magnetic resonance (NMR) spectra were recorded on a Bruker AV300 NMR spectrometer (resonance frequency of 300 MHz for ^{1}H) operated in the Fourier transform mode. $CDCl_3$ and DMSO-d_6 were used as the solvent. Molecular weights and molecular weight distributions were determined by GPC using a series of two linear Styragel columns (HR2 and HR4) and an oven temperature of 45 °C. Waters 1515 pump and Waters 2414 differential refractive index detector (set at 30 °C) were used. The eluent was THF at a flow rate of 1.0 mL/min. A series of six polystyrene standards with molecular weights ranging from 800 to 400 000 g/mol were used for calibration. Fourier transform infrared (FT-IR) spectra were recorded on a Bruker VECTOR-22 IR spectrometer. The spectra were collected over 64 scans with a spectral resolution of 4 cm^{-1}. Dynamic laser light scattering (DLS) measurements were conducted on a commercial spectrometer (ALV/DLS/SLS-5022F) equipped with a multitau digital time correlator (ALV5000) and a cylindrical 22 mW UNIPHASE He−Ne laser (λ_0= 632 nm) as the light source. Scattered light was collected at a fixed angle of 90° for duration of ∼5 min. Distribution averages and particle size distributions were computed using cumulants analysis and CONTIN routines. All data were averaged over three measurements. All samples were filtered through 0.45 μm Millipore Acrodisc-12 filters to remove dust. Transmission electron microscopy (TEM) observations were conducted on a Hitachi H-800 electron microscope at an acceleration voltage of 200 kV. The sample for TEM observations was prepared by placing 10 μL of micellar solution on copper grids coated with thin films of Formvar and carbon successively. Confocal laser scanning microscopy (CLSM) images were acquired using a Leica TCS SP5 microscope. HPLC analysis was performed with a Shimadzu HPLC system, equipped with a LC-20AP binary pump, a SPD-20A UV−vis detector, and a Symmetry C18 column. The UV−vis detector was set at 370 nm linked to the software for data analysis. Fluorescence spectra were recorded on a F-4600 (Hitachi) spectrofluorometer. The slit widths were both set at 5 nm for excitation and emission.

RESULTS AND DISCUSSION

Synthesis of Caged Prodrug NBCCPT and Amphiphilic Diblock Copolymers. CPT is a cytotoxic quinoline alkaloid, which inhibits type I topoisomerase through hydrogen bond interactions under the participation of hydroxyl moiety at position 20. Thus, the covalent linkage of this hydroxyl group with other stimuli-cleavable functionalities is expected to cage the antitumor activity of CPT. In this work, photocaged prodrug NBCCPT was synthesized by exploiting photolabile *o*-nitrobenzyl functional moiety to cage the hydroxyl functionality of CPT (Scheme 2). The chemical structure of NBCCPT was verified by ^{1}H NMR (Figure S1) and ^{13}C NMR (Figure S2a) spectra, together with the corresponding peak assignments, and the ESI−MS results (Figure S2b).

Amphiphilic diblock copolymers, P(CL-*g*-CPT)-*b*-P(OEGMA-*co*-MAEBA)-CPT and PCL-*b*-P(OEGMA-*co*-MAEBA-*co*-FA), were synthesized via the combination of ATRP, ROP, and subsequent "click" functionalization techniques (Scheme 3). Hydroxyl-terminated water-soluble *HO*-P(OEGMA-*co*-MAEBA), serving as ROP macroinitiator in the next step, was synthesized at first via ATRP of OEGMA and MAEBA by using HBMP as the initiator. GPC analysis revealed an M_n of 25,600 and an M_w/M_n of 1.21 (Figure 1a). The comonomer molar contents in the copolymer were estimated from monomer conversions as determined from ^{1}H NMR analysis of the reaction mixture before purification. The obtained *HO*-P(OEGMA-*co*-MAEBA) precursor was employed as initiator for the ROP of CL and CL-Br in anhydrous toluene at 85 °C, affording P(CL-*co*-CLBr)-*b*-P(OEGMA-*co*-MAEBA) diblock copolymer.

A typical GPC trace of P(CL-*co*-CLBr)-*b*-P(OEGMA-*co*-MAEBA) is shown in Figure 1b, revealing a monomodal elution peak and a clear shift to the higher molecular weight side compared with the *HO*-P(OEGMA-*co*-MAEBA) precursor, indicating an almost quantitative initiating efficiency of *HO*-P(OEGMA-*co*-MAEBA) macroinitiator. The total DP of P(CL-*co*-CLBr) and CL molar fractions were determined by ^{1}H NMR analysis from the integral ratio of peak *a* at 9.8 ppm (aldehyde protons adjacent to phenyl group) relative to peak *e* at 2.27 ppm (methylene protons of CL moieties) and peak *f* at 4.03 ppm (methyne protons of CL-Br moieties) (Figure 2b). After being treated with sodium azide, amphiphilic diblock copolymer, (PCL-*g*-N_3)-*b*-P(OEGMA-*co*-MAEBA)-N_3, bearing azide moieties within the hydrophobic block and at the hydrophilic chain terminal, was obtained. The presence of azide moieties in (PCL-*g*-N_3)-*b*-P(OEGMA-*co*-MAEBA)-N_3 can be clearly verified by the characteristic infrared absorption peak at ∼2100 cm^{-1} (Figure S3b). P(CL-*g*-CPT)-*b*-P(OEGMA-*co*-MAEBA)-CPT was finally obtained through the click reaction of (PCL-*g*-N_3)-*b*-P(OEGMA-*co*-MAEBA)-N_3 with an excess of NBCCPT in the presence of CuBr/PMDETA catalyst.

The ^{1}H NMR spectrum of the final product is shown in Figure 2c, together with the peak assignments. We can estimate that there exist ∼16 NBCCPT moieties per diblock copolymer chain on the basis of signal integration ratio of peak *a* at 9.8 ppm (aldehyde protons adjacent to the phenyl group) relative to peak *f* at 5.95 ppm (methylene protons of benzyl groups in NBCCPT). The FT-IR spectrum shown in Figure S3c further verified the quantitative azide group transformation and the complete removal of unreacted NBCCPT, as evidenced from the disappearance of characteristic infrared absorption peaks of both azide moieties at ∼2100 cm^{-1} and alkynyl functionalities at ∼2120 cm^{-1}. In addition, GPC analysis of P(CL-*g*-CPT)-*b*-P(OEGMA-*co*-MAEBA)-CPT revealed an obvious shift to the higher MW side compared to that of P(CL-*co*-CLBr)-*b*-P(OEGMA-*co*-MAEBA) (Figure 1c).

On the other hand, PCL-*Br* was employed as ATRP macroinitiator to copolymerize OEGMA, MAEBA, and AzPMA, affording PCL-*b*-P(OEGMA-*co*-MAEBA-*co*-AzPMA) diblock copolymer. The overall DP of P(OEGMA-*co*-MAEBA-*co*-AzPMA) block was determined to be 70 with OEGMA and MAEBA molar fractions being 0.87 and 0.1, as evidenced by ^{1}H NMR analysis from the integral ratio of peak *c* at 3.38 ppm (methyl protons at the terminal of OEGMA units) and *a* at 9.8 ppm (aldehyde protons adjacent to the phenyl group) relative to peak *d* at 2.27 ppm (methylene protons adjacent to ester functionality of the PCL block) (Figure 3a). Finally, PCL-*b*-P(OEGMA-*co*-MAEBA-*co*-FA) was obtained via click reaction of PCL-*b*-P(OEGMA-*co*-MAEBA-*co*-AzPMA) with an excess of *alkynyl*-folate. ^{1}H NMR spectrum recorded for PCL-*b*-P(OEGMA-*co*-MAEBA-*co*-FA) is shown in Figure 3b. The appearance of new signals characteristic of folate moieties in the range of 6.5−8.7 ppm confirmed the successful functionalization. It can be estimated that there exist ∼2.1 FA moieties per PCL-*b*-P(OEGMA-*co*-MAEBA-*co*-FA) diblock chain. A typical GPC trace of PCL-*b*-P(OEGMA-*co*-MAEBA-*co*-FA) diblock copolymer shown in Figure 1d also revealed an almost monomodal elution peak.

In addition, PCL-*b*-P(OEGMA-*co*-MAEBA-*co*-NBD) diblock copolymer was also synthesized for flow cytometry and

dx.doi.org/10.1021/ma400691j | *Macromolecules* 2013, 46, 6243−6256

confocal microscope colocalization experiments. The molar content of NBD moieties in the P(OEGMA-*co*-MAEBA-*co*-NBD) block was determined to be ~1.0 mol % based on a standard fluorescence calibration curve. The overall DP of P(OEGMA-*co*-MAEBA-*co*-NBD) block was determined to be ~80 with OEGMA and MAEBA molar fractions being 0.56 and 0.43, respectively, as determined by ^{1}H NMR spectrum from the integral ratio of peak *e* at 3.38 ppm (methyl protons at the terminal of OEGMA units) and *c* at 9.8 ppm (aldehyde protons adjacent to the phenyl group) relative to peak *d* at 4.07 ppm (methylene protons adjacent to ester functionality of PCL block) (Figure S4a). Fluorescence excitation and emission spectra recorded for PCL-*b*-P(OEGMA-*co*-MAEBA-*co*-NBD) micelles in aqueous media are shown in Figure S4b.

Fabrication of FA-Decorated and Photocaged Drug Conjugated SCL Micelles. Cancer cell-targeted SCL micelles were fabricated by adding NH_4OAc buffer solution dropwise into the mixed solution of PCL-*b*-P(OEGMA-*co*-MAEBA-*co*-FA) and P(CL-*g*-CPT)-*b*-P(OEGMA-*co*-MAEBA)-CPT diblock copolymers (1/4, w/w) in DMSO under vigorous stirring, affording noncross-linked (NCL) micelles with hydrophobic cores conjugated with photocaged CPT prodrug and hydrophilic coronas containing pendant aldehyde functionalities and FA moieties (Scheme 1). For the fabrication of dynamic covalent SCL micelles, disulfide-containing dihydrazide cross-linker (DTP) was employed, which can react with aldehyde moieties to generate acylhydrazone linkages within hydrophilic coronas. Thus, the cross-linking motif, containing acylhydrazone and disulfide moieties, is cleavable in response to mildly acidic pH and reductive microenvironments, respectively, resulting in de-cross-linking of SCL micelles (Scheme 1).

As revealed by DLS analysis (Figure 4a), both NCL micelles and SCL micelles exhibit an intensity-average hydrodynamic radius, $\langle R_h \rangle$, of 32.6 and 26.8 nm, respectively. It can be clearly observed that the R_h distribution curve shifts to smaller values after the shell cross-linking reaction. In addition, the mixed NCL micelles possess an apparent molar mass, $M_{w,app}$, of ~4.66 × 10^6 g mol^{-1}. Thus, we can approximately calculate that on average, each NCL micelle contains ~433 FA moieties. Although the number of FA moieties on each mixed micelle will vary considerably and exhibit a normal distribution, the probability of existence of micelles bearing no FA ligands at the micellar surface will be extremely low. TEM technique was also employed to characterize mixed block copolymer micelles before and after shell cross-linking. Typical TEM images obtained by drying the aqueous dispersion of NCL micelles and SCL micelles revealed the presence of fairly monodisperse spherical nanoparticles (Figure 5). The number-average diameters of NCL micelles and SCL micelles were determined to be ~36 ± 5 nm and 32 ± 3 nm, respectively. It is well-known that the TEM technique determines nanoparticle dimensions in the dry state, whereas DLS reports intensity-average dimensions in the water-swollen state (especially for corona chains). Moreover, POEGMA micellar coronas are typical invisible under TEM observations due to their low electron contrast. Thus, micellar sizes determined by DLS reasonably agree with those by TEM (Figure 4a).

To further verify the formation of structurally stable SCL micelles, micellar solution after the shell cross-linking procedure was freeze-dried and then dispersed into an organic solvent (THF), which is a good solvent for both blocks. As shown in Figure 4b, the R_h distribution curve recorded for SCL micelles in THF exhibited a monomodal distribution with an

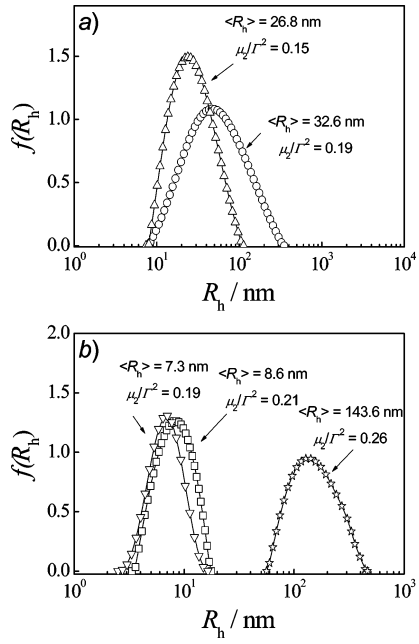

Figure 4. Hydrodynamic radius distributions, $f(R_h)$, recorded for (a) 0.1 g/L aqueous solution of (○) NCL micelles and (Δ) SCL micelles, fabricated from a mixture of PCL-*b*-P(OEGMA-*co*-MAEBA-*co*-FA) and P(CL-*g*-CPT)-*b*-P(OEGMA-*co*-MAEBA)-CPT diblock copolymers (1/4, w/w) in PBS buffer at pH 7.4, and (b) 2.0 g/L SCL micelles (☆) in THF, (▽) upon treating with TCEP in THF, and (□) upon treating with TFA in THF.

$\langle R_h \rangle$ of 143.6 nm and μ_2/Γ^2 of 0.26. This convincingly confirmed that SCL micelles were successfully fabricated and the structural integrity can be maintained after cross-linking; otherwise, diblock copolymer micelles will dissociate into unimers.

As described above, the cross-linking reaction was achieved upon introduction of DTP, thus, the coronas of SCL micelles contain disulfide and acylhydrazone cross-linking motifs, which should exhibit reductive and acidic milieu-triggered cleavage features. To confirm this, the THF dispersion of lyophilized SCL micelles was then treated with an excess of TCEP, which can facilely cleave disulfide bonds. DLS result shown in Figure 4b exhibits an $\langle R_h \rangle$ of 7.3 nm and a μ_2/Γ^2 of 0.19, indicating that SCL micelles were cleaved into molecularly dissolved unimers chains. Comparable results were also obtained for SCL micelles upon treating with trifluoroacetic acid (TFA), which can cleave acylhydrazone linkages (Figure 4b). In addition, Ellmann's reagent was also employed to determine sulfhydryl content within SCL micelles by employing procedures reported previously. The analysis revealed that ~86.6% DTP cross-linker was involved during the cross-linking reaction at a feed molar ratio, DTP/MAEBA, of 1/2, indicating a high apparent degree of shell cross-linking.

Photo-Triggered Cleavage of Conjugated CPT Drug and Dually Modulated Drug Release from SCL Micelles. As described above, DTP cross-linker was utilized to cross-link hydrophilic coronas of NCL micelles, and the obtained SCL micelles covalently anchored with photocaged CPT prodrug in the hydrophobic cores contain cross-linking motifs which are dually responsive to mildly acidic pH and reductive conditions. We envisioned that this new type of design can effectively avoid premature drug leakage during blood circulation due to the covalent nature of drug−polymer backbone linkages. This is in

dx.doi.org/10.1021/ma400691j | *Macromolecules* 2013, 46, 6243−6256

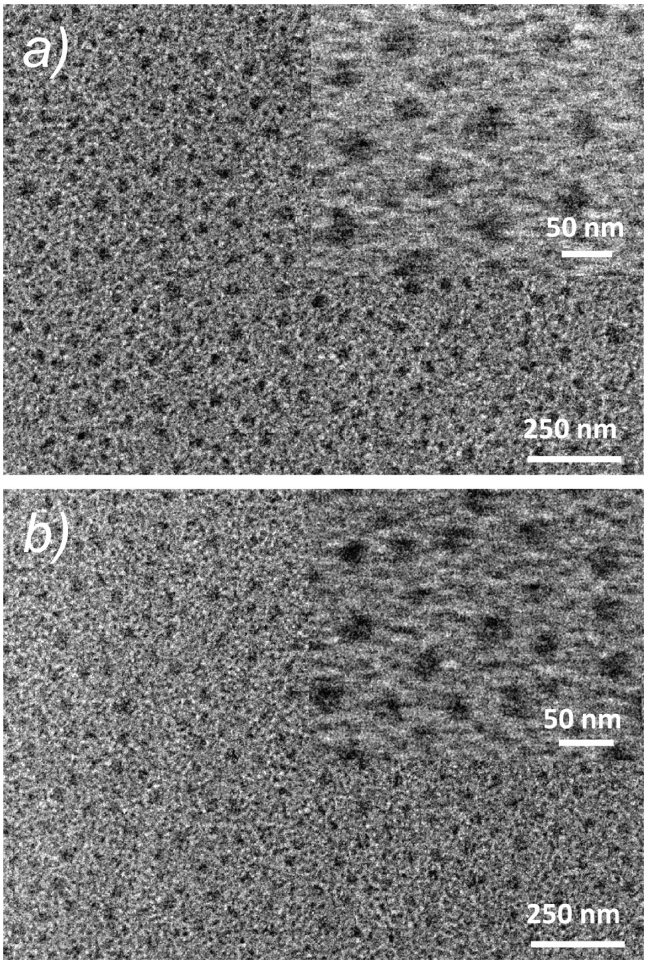

Figure 5. TEM images obtained by drying on copper grids the aqueous dispersion of (a) NCL micelles and (b) SCL micelles fabricated from PCL-*b*-P(OEGMA-*co*-MAEBA-*co*-FA) and P(CL-*g*-CPT)-*b*-P(OEGMA-*co*-MAEBA)-CPT (1/4, w/w) diblock copolymers (inset: magnification of the corresponding TEM image).

contrast to the conventional physical encapsulation system. On the other hand, the cross-linking motif introduced by DTP cross-linker can exhibit reduction and pH dually responsive feature. Thus, upon photocleavage of conjugated CPT drug, the diffusion of active drug into the external media can be further modulated by the cross-linked or de-cross-linked nature of corona networks (Scheme 1).

The drug loading content was determined to be ~10.2 w/w %, as calculated from their molecular structure and the weight ratio between PCL-*b*-P(OEGMA-*co*-MAEBA-*co*-FA) and P(CL-*g*-CPT)-*b*-P(OEGMA-*co*-MAEBA)-CPT diblock copolymers used for the preparation of mixed micelles. Phototriggered cleavage of caged prodrug conjugates to generate active CPT parent drug was then confirmed by high-performance liquid chromatography (HPLC) analysis. As shown in Figure 6, upon UV irradiation of the aqueous solution of P(CL-*g*-CPT)-*b*-P(OEGMA-*co*-MAEBA)-CPT diblock copolymer micelles for various time intervals from 0 to 30 min, the progress of phototriggered CPT release was monitored via signal changes in the HPLC UV channel. With the increase of irradiation duration, the elution peak for the polymer exhibited a slight decrease in intensity, whereas a new peak with increasing intensity, which is corresponding to CPT drug in the active form, emerged in the HPLC elution profile. The above results

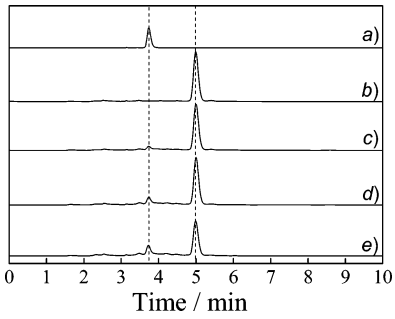

Figure 6. HPLC traces recorded for (a) CPT drug in the effective form and the micellar solution of P(CL-*g*-CPT)-*b*-P(OEGMA-*co*-MAEBA)-CPT diblock copolymer upon UV irradiation for (b) 0 min, (c) 10 min, (d) 20 min, and (e) 30 min with methanol/water (90/10 v/v) as the mobile phase.

revealed that CPT drug can be cleaved from micellar cores via UV irradiation and then diffused out of micellar nanocarriers.

Subsequently, in vitro drug release profiles from FA-decorated and CPT prodrug conjugated NCL and SCL micelles were evaluated at varying conditions. As shown in Figure 7a, the release of CPT parent drug from NCL micelles

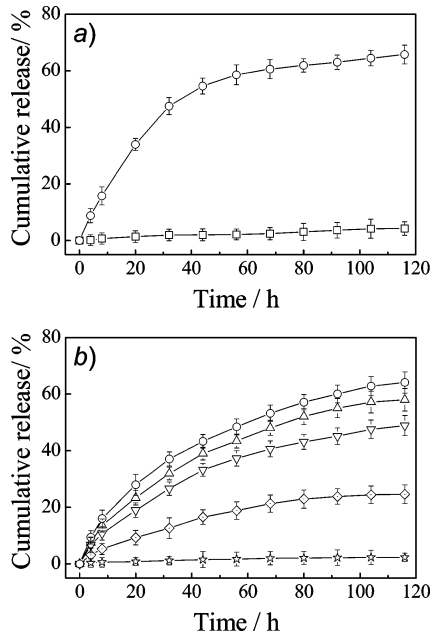

Figure 7. In vitro CPT release profiles recorded for the aqueous solution (0.1 M phosphate buffer, pH 7.4, 37 °C) of (a) NCL micelles (□) without and (○) with UV irradiation for 30 min and (b) SCL micelles (☆) at pH 7.4 without UV irradiation, and (◊) at pH 7.4, (Δ) pH 5.0, and (▽) pH 7.4 with 10 mM DTT and (○) pH 5.0 with 10 mM DTT after UV irradiation for 30 min. Micelles were fabricated from a mixture of PCL-*b*-P(OEGMA-*co*-MAEBA-*co*-FA) and P(CL-*g*-CPT)-*b*-P(OEGMA-*co*-MAEBA)-CPT diblock copolymers (1/4, w/w).

was initiated upon UV irradiation for 30 min, and ~65.8% release of total conjugated CPT can be achieved over ~120 h, whereas only negligible release was exhibited by NCL micelles without UV irradiation. This can be surely ascribed to the covalent linkage nature between CPT and polymer backbones within micellar cores. Only upon subjected to UV irradiation, those covalent linkages can be cleaved. As a control, in vitro CPT release profile from SCL micelles subjected with or

dx.doi.org/10.1021/ma400691j | *Macromolecules* 2013, 46, 6243−6256

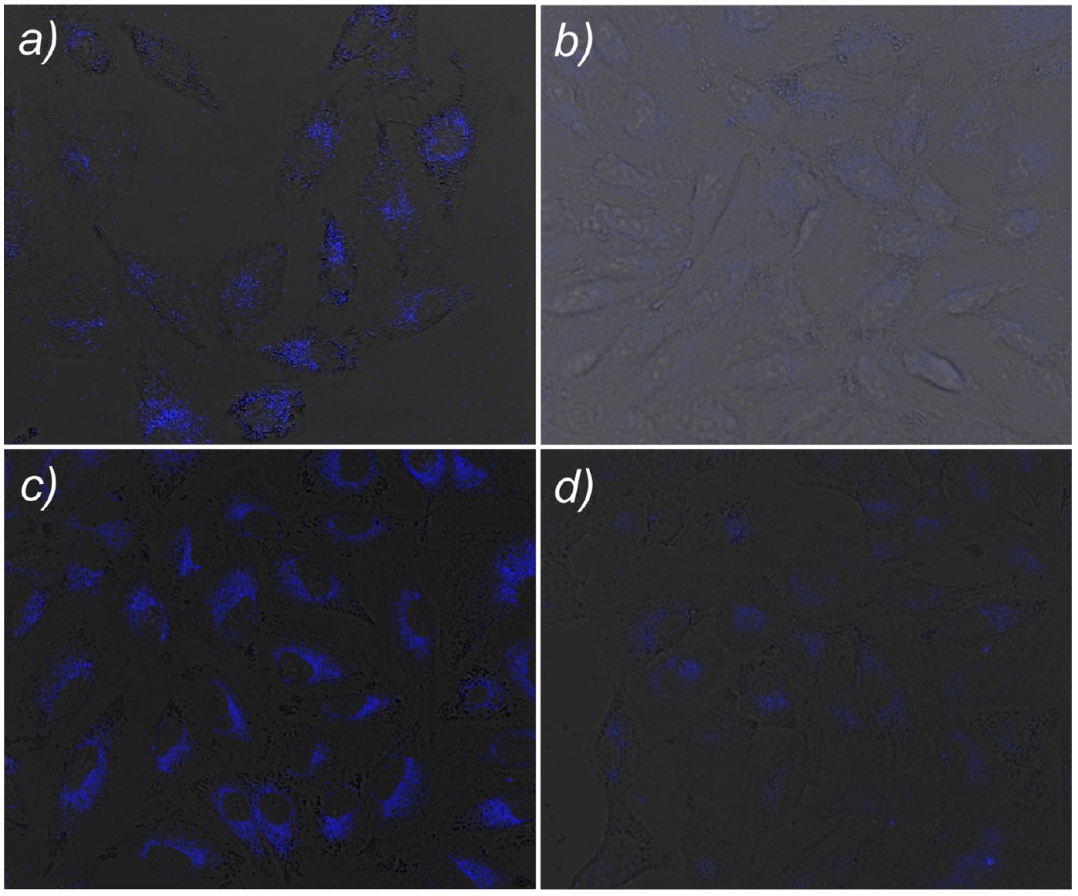

Figure 8. CLSM images recorded for A549 cells after incubation with FA-decorated SCL micelles for 1 h (a) in the absence and (b) presence of free folic acid (~1000-fold excess over folic acid moieties decorated at the surface of SCL micelles). A549 cells after 2 h incubation with (c) FA-decorated SCL micelles and (d) FA-free SCL micelles.

without UV irradiation is shown in Figure 7b. Again, negligible CPT release from SCL micelles at pH 7.4 without irradiation was observed. Within 24 h, SCL micelles at pH 7.4 without UV irradiation exhibited only ~1.2% release of conjugated CPT drug, whereas ~11% CPT was released for SCL micelles after UV irradiation over ~24 h. These results revealed that the "photocaging strategy" can almost completely block premature drug leakage, which are typically encountered in conventional physical encapsulation systems.

A comparison between parts a and b of Figure 7 further revealed that for both NCL micelles and SCL micelles upon UV irradiation, ~65.8% and ~22% of conjugated CPT drug can be released over a period of 120 h, respectively. Decreased CPT release for SCL micelles as compared to that of NCL micelles must be due to the corona cross-linked nature in the form. Cross-linking of micellar coronas will pose physical barriers for the diffusion of CPT from micelles upon the cleavage of covalent linkages between CPT and polymer backbones. On the other hand, the dually responsive (mildly acidic and reductive milieu) nature of DTP cross-linker used for the fabrication of SCL micelles can be further exploited for external stimuli-tunable CPT release. This is especially intriguing considering that both mildly acidic and reductive milieu are biologically relevant to intracellular endosomes/lysosomes organelles and cytosol, respectively.

We then explored CPT release profiles for SCL micelles upon UV irradiation and followed by incubating under varying solution conditions (mildly acidic pH and/or reductive conditions; Figure 7b). After UV irradiation of SCL micelles, it was found that although significant acceleration of CPT release can be actuated upon either introducing 10 mM DTT or adjusting the solution pH to 5.0, the most rapid release was achieved when dual stimuli were applied simultaneously. In the latter case, i.e., at pH 5.0 in the presence of 10 mM DTT, the drug release profile is quite comparable to that of NCL micelles as shown in Figure 7a. As reported in previous literatures, the hydrolysis and exchange of acylhydrazone bonds are active enough at pH 5.0, eventually leading to their partial cleavage. In addition, reductive environments such as those induced by high thiol levels can reduce disulfide bonds into thiol moieties. Since both cleavage reactions are equilibrium ones, thus, it is quite reasonable to deduce that DTP cross-linking bonds will cleave most effectively under both mildly acidic pH and reductive conditions. The above results implied that FA-decorated and CPT prodrug conjugated SCL micelles are capable of maintaining their structural integrity and completely prohibiting premature drug leakage during blood circulation (i.e., under neutral pH and low thiol level); whereas upon cellular uptake via FA receptor-mediated endocytosis and subsequent UV irradiation to cleave photocaged linkages, enhanced CPT release can be achieved both in acidic organelles (e.g., endosomes and lysosomes) and in the cytosol after endosomal/lysosomal escape (Scheme 1).

Cellular Uptake and In Vitro Cytotoxicity of SCL Micelles. The cellular uptake of FA-decorated SCL micelles by the folate receptor-positive cell line, A549 cells, was investigated

dx.doi.org/10.1021/ma400691j | *Macromolecules* 2013, 46, 6243−6256

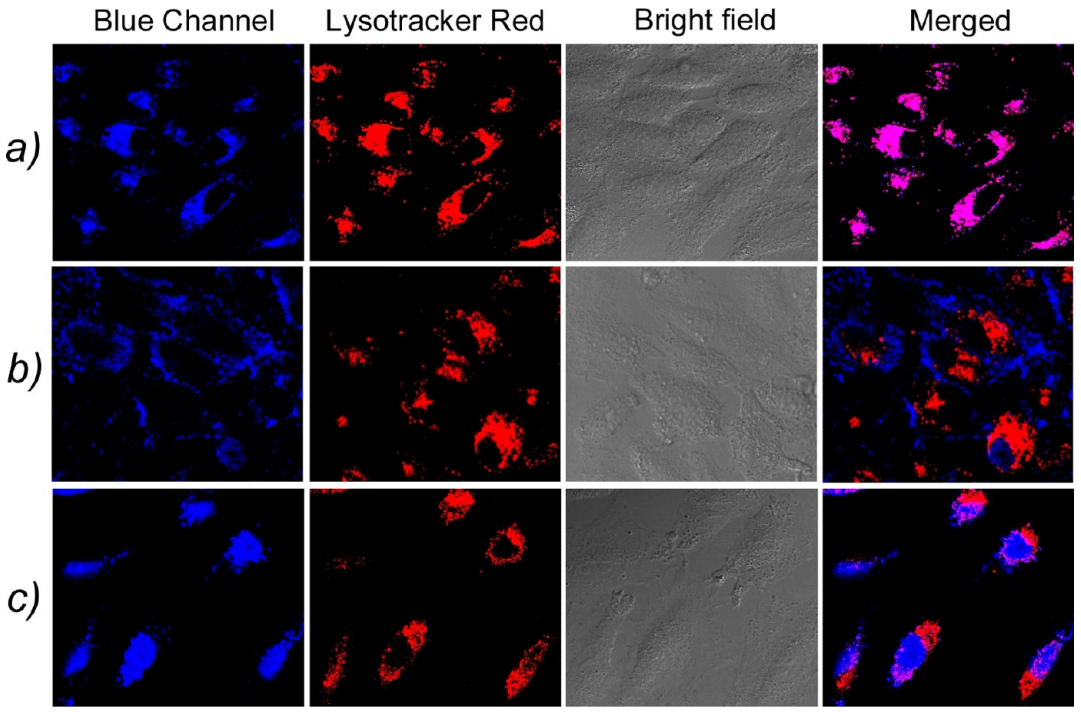

Figure 9. CLSM images recorded for A549 cells after incubation with FA-decorated SCL micelles for (a) 4 h, (b) 8 h, and (c) 12 h in total. Cells were first incubated with FA-decorated SCL micelles at 37 °C for 2 h, followed by UV irradiation for 15 min, then incubated for another 2, 6, and 10 h, respectively. Late endosomes/lysosomes were stained with Lysotracker Red (red).

by confocal laser scanning microscopy (CLSM) and compared with FA-free SCL micelles to probe the effect of targeting ligand on the cellular uptake efficiency. Since CPT itself is fluorescent, its emission was used directly to visualize cellular uptake without additional fluorescence labeling. Therefore, the fluorescence intensity should in principle be proportional to the amount of CPT-conjugated SCL micelles internalized by cells. As shown in parts a and b of Figure 8, after incubation with FA-decorated SCL micelles for 1 h, substantial cellular internalization into A549 cell cytoplasm was observed; however, upon addition of competitive free folic acid (~1000-fold excess over folic acid moieties decorated at the surface of SCL micelles), cellular internalization events were almost completely prohibited. Thus, competitive assay with free folic acid further confirmed the FA receptor-mediated endocytic pathway. As shown in parts c and d of Figure 8, CLSM images of A549 cells incubated with FA-decorated SCL micelles exhibited higher fluorescence intensity compared to FA-free SCL micelles over the same incubation duration (~2 h).

Further internalization studies were performed by employing the flow cytometry technique in order to acquire more quantitative data. As shown in Figure S5, A549 cells were incubated with NBD dye-labeled and FA-decorated or FA-free SCL micelles for 1 h at 4 and 37 °C, respectively. Cells without micellar nanoparticle coincubation were used as a negative control and showed only autofluorescence of the cells. For A549 cells incubated at 4 °C with either FA-decorated or FA-free SCL micelles, no obvious fluorescence enhancement was observed, revealing that the cellular uptake of SCL micelles followed an energy-dependent pathway. Whereas at 37 °C, cells incubated with FA-decorated SCL micelles showed much higher fluorescence intensity, as compared to those with FA-free SCL micelles. These results suggested that cellular uptake of SCL micelles can be considerably enhanced by covalently attaching FA onto the hydrophilic shell and that FA-decorated SCL micelles can be transported into A549 cells via the receptor mediated endocytosis process (Scheme 1).

To verify whether SCL micellar nanocarriers can escape from endosomes/lysosomes with the capability of CPT delivery, A549 cells were first incubated with FA-decorated SCL micelles for 2 h to ensure sufficient cellular uptake, followed by irradiation for 15 min, and then with another 2 h, 6 and 10 h of incubation. As shown in Figure 9, confocal laser microscopic observations indicated that after 4 h incubation in total, FA-decorated SCL micelles were mainly colocalized with Lysotracker Red, suggesting that SCL micelles resided in late endosomes and/or lysosomes. However, upon incubation with FA-decorated SCL micelles for 8 h, the separate localization of red and blue fluorescence with minimal colocalization inside cells is clearly evident, confirming that micellar nanocarriers should have escaped from lysosomal vesicles and entered into the cytosol. The colocalization ratios were calculated to be 89.3% for 4 h and 23.6% for 8 h (total incubation duration). We also conducted colocalization experiments for A549 cells upon 8 h incubation with FA-decorated SCL micelles, but without UV irradiation. Quite comparable extent of localization separation between red and blue fluorescent dots was observed with the colocalization ratio determined to be ~27.3%. Thus, it is reasonable for us to rule out the possibility of UV irradiation-induced endosomal escape for SCL micelles.

In the above experiment, CPT prodrugs conjugated within micellar cores also serve as fluorescent labeling of nanocarriers. There also exists the possibility that the blue channel fluorescence emission was due to free CPT cleaved from polymer chains (Figure 9), instead of CPT-conjugated micellar nanocarriers. To further interrogate the endosomal escaping capability of SCL micelles, colocalization experiments were also conducted with NBD-labeled SCL micelles fabricated from a

dx.doi.org/10.1021/ma400691j | *Macromolecules* 2013, 46, 6243−6256

mixture of PCL-*b*-P(OEGMA-*co*-MAEBA-*co*-FA) and PCL-*b*-P(OEGMA-*co*-MAEBA-*co*-NBD) (Figure S6). After 4, 8, and 12 h incubation with NBD-labeled SCL micelles, the colocalization ratios were determined to be 87.6%, 31.6%, and 27.9%, respectively. These results agreed quite well with those shown in Figure 9 and further confirmed that FA-decorated and drug-conjugated SCL micelles possessed considerable endosomal escaping ability.

CPT is one type of DNA-toxin, which target nuclear DNA to inhibit topoisomerase involved in DNA replication to induce cell apoptosis; thus, CPT has to localize within the nucleus to induce pharmacological responses. It is encouraging to find that upon cellular uptake and UV irradiation for 15 min, followed by incubation for 10 h (in total 12 h incubation), very intense blue fluorescence was observed within the nucleus, as compared to that in the cytoplasm (Figure 9c). Interestingly, NBD-labeled drug-free SCL micelles did not enter cell nucleus even after 12 h coincubation with A549 cells (Figure S6c). These results clearly indicate that effective drug cleavage from SCL micellar cores occurred after photoactivation, and this is accompanied by subsequent endosomal escape and efficient nuclear accumulation of bioactive CPT drug.

The cytotoxic effects of CPT parent drug, FA-decorated SCL micelles, and FA-free SCL micelles against cultured HepG2 cells and A549 cells were then evaluated using the MTT assay. HepG2 cells are human hepatoma cells without overexpressed FA receptors, whereas A549 cells are human lung carcinoma cells that express FA receptors.[51] Figure 10A shows the HepG2 cell viability in the presence of CPT parent drug, FA-decorated SCL micelles, and FA-free SCL micelles with and without UV irradiation. No significant differences in the viability of HepG2 cells can be observed when cultured with FA-decorated SCL micelles and FA-free SCL micelles, indicating that the cytotoxicity of SCL micelles with or without FA ligands were comparable against HepG2 cells (e versus f in Figure 10A). This observation is reasonable considering that HepG2 cells lack over-expressed folate receptors.

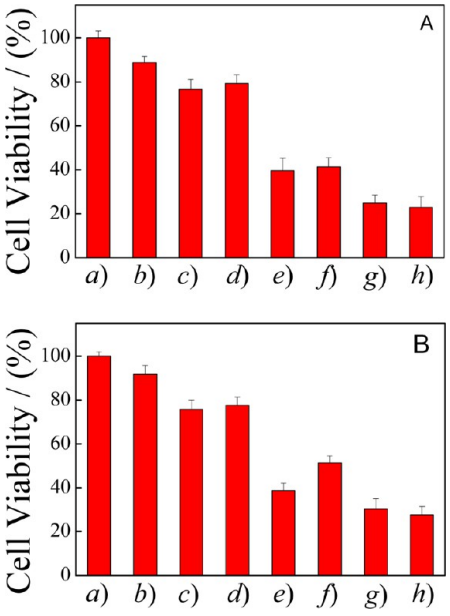

Figure 10. Viability of (A) HepG2 cells and (B) A549 cells administered with (a) control, (b) UV irradiation, (c) FA-decorated SCL micelles, (d) FA-free SCL micelles, (e) FA-decorated SCL micelles upon UV irradiation, (f) FA-free SCL micelles upon UV irradiation, (g) CPT drug in the effective form, and (h) CPT parent drug upon UV irradiation (irradiation time, 15 min; incubation time, 36 h; CPT equivalent dosage, 5 μg mL^{-1}).

Figure 10B shows the cytotoxicity of FA-decorated SCL micelles, FA-free SCL micelles, and CPT parent drug against A549 cells. The cell viability in the presence of FA-decorated SCL micelles was obviously lower than that with FA-free SCL micelles (e versus f in Figure 10B). This result reveals that FA-targeting ligands present on the surface of FA-decorated SCL micelles play an important role in enhancing the cytotoxicity by promoting surface binding and cellular entry via receptor-mediated endocytosis mechanism (Scheme 1). Data shown in Figure 10 also suggest that UV irradiation for 15 min is not by itself detrimental to cells, and it will also not affect the cytotoxicity of free CPT drug (a versus b, g versus h in Figure 10). In addition, phototriggered enhancement of cytotoxicity against both types of cells for NCL and SCL micelles can be clearly discerned (c versus e, d versus f in Figure 10).

Finally, cell viability against A549 cells upon incubation with CPT parent drug, FA-decorated NCL or SCL micelles as a function of CPT-equivalent concentration is shown in Figure 11. Cells were pretreated with the aqueous dispersion of either

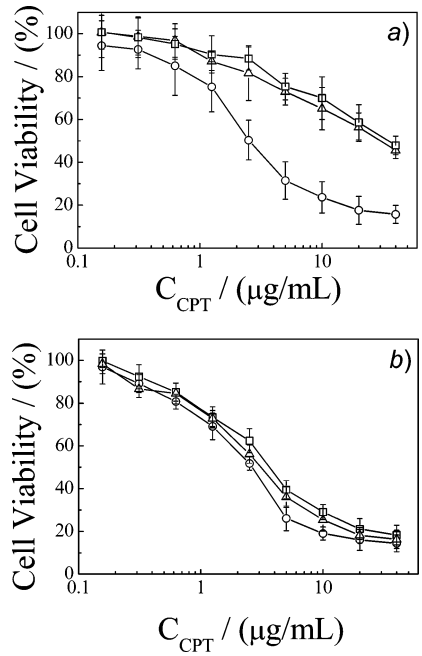

Figure 11. Viability of A549 cells (a) without UV irradiation and (b) upon UV irradiation for 15 min after cellular uptake of (Δ) FA-decorated NCL micelles, (□) FA-decorated SCL micelles, and (○) CPT parent drug, and then incubating for another 36 h at varying equivalent CPT concentrations.

CPT parent drug or CPT-conjugated NCL or SCL micelles decorated with FA targeting ligands at varying concentrations, then irradiated for 15 min or kept in the dark as a control, and finally incubated in the dark for another 36 h, as shown in Figure 11. CPT parent drug as a control, with and without irradiation, gave similar dose−response curves with IC_{50} values being ~2.54 and ~2.63 μg mL^{-1}, respectively. On the other hand, NCL and SCL micelles without irradiation exhibited minimal toxicity to cells, presenting IC_{50} values of ~29.2 and ~34.1 μg mL^{-1}, respectively. This observation indicates that the

dx.doi.org/10.1021/ma400691j | *Macromolecules* 2013, 46, 6243−6256

photocaged nature of CPT parent drug within micellar cores and the hydrophilic outer corona can effectively shield the cytotoxicity of micellar nanocarriers. Surprisingly, UV irradiation can greatly enhance the cytotoxicity of CPT prodrug conjugated NCL and SCL micelles with IC_{50} values being ~3.0 and ~3.5 $\mu g\ mL^{-1}$, respectively. Compared with nonirradiated samples, irradiated ones exhibited at least ~9.7-fold increase in toxicity upon photoinduced drug decaging and release.

CONCLUSIONS

In summary, we fabricated FA-decorated dually responsive SCL micelles conjugated with photocaged CPT prodrug in hydrophobic cores from a mixture of amphiphilic diblock copolymers, which were functionalized with targeting ligands and caged CPT drug in the hydrophilic and hydrophobic domains, respectively. The obtained FA-decorated and caged CPT conjugated SCL micelles contain disulfide and acylhydrazone linkages in the cross-linking motif, thus exhibiting reduction and pH dually responsive de-cross-linking feature. Premature drug leakage can be efficiently prohibited under physiological conditions due to the covalent conjugation of CPT drug and diffusion barrier exerted by cross-linked micellar coronas, whereas accelerated drug release can be achieved under mildly acidic and/or reductive microenvironment upon phototriggered cleavage of caged CPT prodrug moieties. Cell culture studies confirmed that the extent of A549 cellular uptake for FA-decorated SCL micelles was more prominent than FA-free SCL micelles, thereby demonstrating higher cytotoxicity against A549 cells. FA-decorated SCL micelles also exhibited excellent endosomal escape capability, resulting in considerable nucleic accumulation of chemotherapeutic drug. Finally, SCL micelles without irradiation exhibited minimal toxicity to cells, whereas at least ~9.7-fold enhanced cytotoxicity can be achieved upon irradiation. The SCL micellar cores can also encapsulate other hydrophobic drugs to further achieve combination chemotherapy. Overall, the reported cancer cell-targeting and multiresponsive SCL micelles covalently conjugated with caged chemotherapeutic drugs augurs well for their promising applications in the field of targeted drug delivery. In addition, the modularity of this platform allows for further integration with more versatile targeting ligands, new bioresponsive linkages, and novel drug caging and decaging strategies such as near-infrared (NIR)-cleavable prodrug linkages.

ASSOCIATED CONTENT

Supporting Information

^1H NMR, ^{13}C NMR, and ESI−MS characterization data of NBCCPT prodrug, FT-IR spectra, flow cytometry, and additional confocal microscope colocalization results. This information is free of charge via the Internet at http://pubs.acs.org/.

AUTHOR INFORMATION

Corresponding Author

*E-mail: (S.L.) sliu@ustc.edu.cn.

Notes

The authors declare no competing financial interest.

ACKNOWLEDGMENTS

The financial support from the National Natural Scientific Foundation of China (NNSFC) Project (21274137, 51273190, 91027026 and 51033005), Fundamental Research Funds for the Central Universities, and Specialized Research Fund for the Doctoral Program of Higher Education (SRFDP, 20123402130010) is gratefully acknowledged.

REFERENCES

(1) Peer, D.; Karp, J. M.; Hong, S.; Farokhzad, O. C.; Margalit, R.; Langer, R. *Nature Nanotechnol.* **2007**, *2*, 751−760.
(2) Xiong, X.-B.; Falamarzian, A.; Garg, S. M.; Lavasanifar, A. *J. Controlled Release* **2011**, *155*, 248−261.
(3) Hu, J. M.; Zhang, G. Q.; Liu, S. Y. *Chem. Soc. Rev.* **2012**, *41*, 5933−5949.
(4) Thurmond, K. B.; Kowalewski, T.; Wooley, K. L. *J. Am. Chem. Soc.* **1996**, *118*, 7239−7240.
(5) Read, E. S.; Armes, S. P. *Chem. Commun.* **2007**, 3021−3035.
(6) O'Reilly, R. K.; Hawker, C. J.; Wooley, K. L. *Chem. Soc. Rev.* **2006**, *35*, 1068−1083.
(7) Xu, X. W.; Flores, J. D.; McCormick, C. L. *Macromolecules* **2011**, *44*, 1327−1334.
(8) Hu, X.; Li, H.; Luo, S.; Liu, T.; Jiang, Y.; Liu, S. *Polym. Chem.* **2013**, *4*, 695−706.
(9) Ding, J. F.; Liu, G. J. *Macromolecules* **1998**, *31*, 6554−6558.
(10) Li, Y.; Lokitz, B. S.; Armes, S. P.; McCormick, C. L. *Macromolecules* **2006**, *39*, 2726−2728.
(11) Jiang, X. Z.; Ge, Z. S.; Xu, J.; Liu, H.; Liu, S. Y. *Biomacromolecules* **2007**, *8*, 3184−3192.
(12) Jiang, X. Z.; Zhang, G. Y.; Narain, R.; Liu, S. Y. *Langmuir* **2009**, *25*, 2046−2054.
(13) Jiang, X. Z.; Zhang, J. Y.; Zhou, Y. M.; Xu, J.; Liu, S. Y. *J. Polym. Sci., Part A: Polym. Chem.* **2008**, *46*, 860−871.
(14) Li, C.; Wallace, S. *Adv. Drug Delivery Rev.* **2008**, *60*, 886−898.
(15) Khandare, J.; Minko, T. *Prog. Polym. Sci.* **2006**, *31*, 359−397.
(16) Liu, T.; Li, X. J.; Qian, Y. F.; Hu, X. L.; Liu, S. Y. *Biomaterials* **2012**, *33*, 2521−2531.
(17) Pirrung, M. C. *Chem. Rev.* **1997**, *97*, 473−488.
(18) Li, Z.; Bai, X.; Ruparel, H.; Kim, S.; Turro, N. J.; Ju, J. *Proc. Natl. Acad. Sci. U.S.A.* **2003**, *100*, 414−419.
(19) Garcia-Garibay, M. A. *J. Am. Chem. Soc.* **2012**, *134*, 8289−8292.
(20) Lal, S.; Clare, S. E.; Halas, N. J. *Acc. Chem. Res.* **2008**, *41*, 1842−1851.
(21) Barltrop, J. A.; Plant, J.; Schofield, P. *Chem. Commun.* **1966**, 822−823.
(22) Patchornik, A.; Amit, B.; Woodward, R. B. *J. Am. Chem. Soc.* **1970**, *92*, 6333−6335.
(23) Zhao, H.; Sterner, E. S.; Coughlin, E. B.; Theato, P. *Macromolecules* **2012**, *45*, 1723−1736.
(24) Zhang, Z.; Hatta, H.; Ito, T.; Nishimoto, S. *Org. Biomol. Chem.* **2005**, *3*, 592−596.
(25) Agasti, S. S.; Chompoosor, A.; You, C.-C.; Ghosh, P.; Kim, C. K.; Rotello, V. M. *J. Am. Chem. Soc.* **2009**, *131*, 5728−5729.
(26) Dcona, M. M.; Mitra, D.; Goehe, R. W.; Gewirtz, D. A.; Lebman, D. A.; Hartman, M. C. T. *Chem. Commun.* **2012**, *48*, 4755−4757.
(27) Ki Choi, S.; Thomas, T.; Li, M.-H.; Kotlyar, A.; Desai, A.; Baker, J. J. R. *Chem. Commun.* **2010**, *46*, 2632−2634.
(28) Johnson, J. A.; Lu, Y. Y.; Burts, A. O.; Lim, Y.-H.; Finn, M. G.; Koberstein, J. T.; Turro, N. J.; Tirrell, D. A.; Grubbs, R. H. *J. Am. Chem. Soc.* **2010**, *133*, 559−566.
(29) Johnson, J. A.; Lu, Y. Y.; Burts, A. O.; Xia, Y.; Durrell, A. C.; Tirrell, D. A.; Grubbs, R. H. *Macromolecules* **2010**, *43*, 10326−10335.
(30) Georgianna, W. E.; Lusic, H.; McIver, A. L.; Deiters, A. *Bioconj. Chem.* **2010**, *21*, 1404−1407.
(31) Jain, P. K.; Karunakaran, D.; Friedman, S. H. *Angew. Chem., Int. Ed.* **2013**, *52*, 1404−1409.
(32) Fan, N.-C.; Cheng, F.-Y.; Ho, J.-a. A.; Yeh, C.-S. *Angew. Chem., Int. Ed.* **2012**, *51*, 8806−8810.
(33) Tanabe, K.; Nakata, H.; Mukai, S.; Nishimoto, S.-i. *Org. Biomol. Chem.* **2005**, *3*, 3893−3897.

(34) Zhao, Y.; Zheng, Q.; Dakin, K.; Xu, K.; Martinez, M. L.; Li, W.-H. *J. Am. Chem. Soc.* **2004**, *126*, 4653−4663.
(35) Pawle, R. H.; Eastman, V.; Thomas, S. W. *J. Mater. Chem.* **2011**, *21*, 14041−14047.
(36) Wu, N.; Deiters, A.; Cropp, T. A.; King, D.; Schultz, P. G. *J. Am. Chem. Soc.* **2004**, *126*, 14306−14307.
(37) Farokhzad, O. C.; Langer, R. *ACS Nano* **2009**, *3*, 16−20.
(38) Maeda, H. *Bioconj. Chem.* **2010**, *21*, 797−802.
(39) Kamaly, N.; Xiao, Z.; Valencia, P. M.; Radovic-Moreno, A. F.; Farokhzad, O. C. *Chem. Soc. Rev.* **2012**, *41*, 2971−3010.
(40) Elnakat, H.; Ratnam, M. *Adv. Drug Delivery Rev.* **2004**, *56*, 1067−1084.
(41) Kamen, B. A.; Smith, A. K. *Adv. Drug Delivery Rev.* **2004**, *56*, 1085−1097.
(42) Giovanella, B. C.; Harris, N.; Mendoza, J.; Cao, Z.; Liehr, J.; Stehlin, J. S. *Ann. N.Y. Acad. Sci.* **2000**, *922*, 27−35.
(43) O'Leary, J.; Muggia, F. M. *Eur. J. Cancer* **1998**, *34*, 1500−1508.
(44) Zhao, H.; Gu, W.; Sterner, E.; Russell, T. P.; Coughlin, E. B.; Theato, P. *Macromolecules* **2011**, *44*, 6433−6440.
(45) Xu, N.; Wang, R.; Du, F.-S.; Li, Z.-C. *J. Polym. Sci., Part A: Polym. Chem.* **2009**, *47*, 3583−3594.
(46) Wolf, F. F.; Friedemann, N.; Frey, H. *Macromolecules* **2009**, *42*, 5622−5628.
(47) Liu, T.; Qian, Y.; Hu, X.; Ge, Z.; Liu, S. *J. Mater. Chem.* **2012**, *22*, 5020−5030.
(48) De, P.; Gondi, S. R.; Sumerlin, B. S. *Biomacromolecules* **2008**, *9*, 1064−1070.
(49) Uchiyama, S.; Matsumura, Y.; de Silva, A. P.; Iwai, K. *Anal. Chem.* **2003**, *75*, 5926−5935.
(50) Kumar, S.; Dory, Y. L.; Lepage, M.; Zhao, Y. *Macromolecules* **2011**, *44*, 7385−7393.
(51) Santra, S.; Kaittanis, C.; Santiesteban, O. J.; Perez, J. M. *J. Am. Chem. Soc.* **2011**, *133*, 16680−16688.